Toward single particle reconstruction without particle picking: Breaking the detection limit

Tamir Bendory, Nicolas Boumal, William Leeb and Amit Singer

May 25, 2018

Abstract

Here comes the abstract

1 Introduction

[Revise–Cryo–electron microscopy (cryo–EM) is an innovative technology for single particle reconstruction (SPR) of macromolecules.] In a cryo–EM experiment, biological samples are rapidly frozen in a thin layer of vitreous ice. Within the ice, the molecules are randomly oriented and positioned. The microscope produces a 2D image of the samples embedded in the ice called a *micrograph*. Each micrograph contains tomographic projections of the samples at unknown locations and under unknown viewing directions. The goal is to construct 3-D models of the molecules from the micrographs.

The signal to noise ratio (SNR) of the projections in the micrographs is a function of two dominating factors. On the one hand, the SNR is a function of the electron dose. To keep radiation damage within acceptable bounds, the dose must be kept low, which leads to high noise levels. On the other hand, the SNR is a function of the molecule size. The smaller the molecules, the fewer detected electrons carry information about them.

All contemporary methods in the field split the reconstruction procedure in several stages. The first stage consists in extracting the various particle projections from the micrographs. This is called *particle picking*. Later stages aim to construct a 3-D model of the molecule from these projections. The quality of the reconstruction eventually hinges on the quality of the particle picking stage. As can be seen from Figure 1, locating the particles becomes increasingly challenging as the SNR degrades.

Crucially, it can be shown that reliable detection of individual particles is impossible below a certain critical SNR. This fact has been recognized early on by the cryo-EM community. In particular, in a highly cited paper from 1995, Henderson [26] investigates the following questions:

> *For the purposes of this review, I would like to ask the question: what is the smallest size of free-standing molecule whose structure can in principle be determined by phase-contrast electron microscopy? Given what has already been demonstrated in published work, this reduces to the question: what is the smallest size of molecule for which it is possible to determine from images of unstained molecules the five*

parameters needed to define accurately its orientation (three parameters) and position (two parameters) so that averaging can be performed?

In that paper and in others that followed (e.g., [20]), it was established that particle picking is impossible for molecules below a certain weight. As a result, it is impossible to reconstruct such small molecules by any of the existing computational pipelines for single particle analysis, as the particles themselves cannot be picked from the micrographs. This has motivated recent technical advances in the field, including the use of Volta phase plates [30, 35] and scaffolding cages [37]. Despite this progress, detecting small molecules (below 50 kDa) in the micrographs remains a challenge.

In this paper, we argue that there is a gap between the two questions in the quoted excerpt above, and that one may be able to exploit it to design better reconstruction algorithms. Specifically, the impossibility of particle picking does not necessarily imply impossibility of particle reconstruction. Indeed, the aim is only to reconstruct the molecule: estimating the locations of the particles in the micrograph is merely a helpful intermediate stage when it can be done. Our main message is that the limits particle packing imposes on molecule size do not translate into limits on particle reconstruction.

As a proof of concept, we study a simplified model where an unknown image appears numerous times at unknown locations in several micrographs, each affected by additive Gaussian noise—see Figure 1 for an illustration. The goal is to estimate the planted image. The task is interesting in particular when the SNR is low enough that particle picking cannot be done reliably. A precise mathematical formulation of the model, including an extension where more than one planted images are to be recovered, is provided in Section 4. To be clear, we do not consider here many prominent features of real SPR experiments and do not aim to reconstruct any 3-D structure. Instead, we solve a simpler problem that we believe captures key elements of the SPR problem. We note that similar models emerge in spike sorting [34], passive radar [21] and system identification [38].

In order to recover the planted image, we use autocorrelation analysis. In a nutshell, we relate the autocorrelation functions of the micrographs to the autocorrelation functions of the planted image. For any noise level, these autocorrelations can be estimated to any desired accuracy provided individual occurrences of the image are well separated and the image appears sufficiently many times in the micrographs. Importantly, there is no need to detect individual occurrences. The autocorrelations of the micrographs are straightforward to compute and require only one pass over the data. These directly yield estimates for the autocorrelations of the image. To estimate the image itself from its estimated autocorrelations, we solve a nonlinear inverse problem via least-squares or a phase retrieval algorithm; see Figure 2 for an illustration and Section 4 for details. As a side note, we mention that expectation-maximization (EM)—a popular framework in SPR—is intractable for this problem; see Appendix C for a discussion.

Another interesting feature of the described approach pertains to model bias, whose importance in cryo-EM was stressed by a number of authors [48, 44, 27, 47]. In the classical "Einstein from noise" experiment, multiple realizations of pure noise are aligned to a picture of Einstein using cross-correlation and then averaged. In [44], it was shown that the averaged noise rapidly becomes remarkably similar to the Einstein template. In the context of cryo–EM, this experiment exemplifies how prior assumptions about the particles may influence the reconstructed structure. This model bias is common to all particle picking methods based on template matching. In our approach, no templates are required.

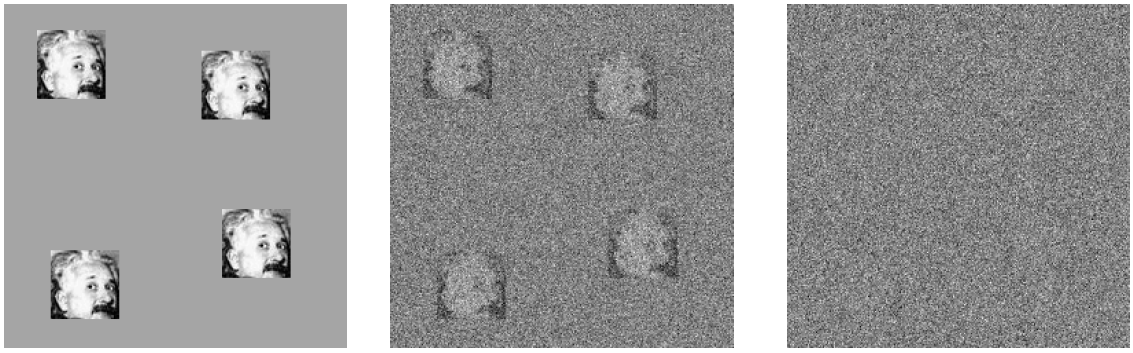

(a) $\sigma = 0$ (b) $\sigma = 0.5$ (c) $\sigma = 3$

Figure 1: Example of micrographs of size 250×250 with additive white Gaussian noise of variance σ^2 for increasing values of σ. Each micrograph contains four occurrences of the same 50×50 image of Einstein. In panel (c), the noise level is such that it is very challenging to locate the occurrences of the planted image. In fact, it can be shown that at low SNR, reliable detection of individual image occurrences is impossible, even if the true image is known. By analogy to cryo-EM, this depicts a scenario where particle picking cannot be done.

2 Results

In this section we describe some numerical experiments and show results. The experimental details and the algorithms are discussed at length in Section 4.

In the first experiment, we estimated Einstein's image of size 50×50 from multiple micrographs of size 4096×4096 pixels, contaminated with additive i.i.d. Gaussian noise with standard deviation $\sigma = 3$ ($\mathsf{SNR} = 1/20$). An illustrative example of a micrograph appears in the right panel of Figure 1. Each micrograph contains multiple occurrences of Einstein's image in random locations, while keeping a separation of 49 pixels between the images in each direction. From the micrographs, we estimated the signal's power spectrum, which is equivalent to the second-order autocorrelation. Then, in order to estimate the signal itself, we applied a standard phase retrieval algorithm called relaxed-reflect-reflect (RRR).

As an initial guess, we picked an image of the physicist Issac Newton; see Figure 2a. If the algorithm was prone to model bias, we would expect to get as an output an image that resembles Newton, similarly to the "Einstein from noise" effect of Figure **??**. However, the experiment exhibits the desired phenomenon: the more data we collect, the better the reconstruction quality.

Figure 2 demonstrates several recovery results for different number of recorded micrographs. Figure 3 presents the normalized recovery error and the power spectrum estimation error as a function of the number of micrographs. To measure the error, we use the root mean square error (RMSE) defined as

$$\mathrm{RMSE} := \frac{\|x - \hat{x}\|_{\mathrm{F}}}{\|x\|_{\mathrm{F}}}, \tag{2.1}$$

where x and $\hat{x}$ are, respectively, the underlying and estimated image, and $\|\cdot\|_{\mathrm{F}}$ stands for the Frobenius norm. As expected, the RMSE of estimating the power spectrum decreases

linearly with slope $-1/2$ in logarithmic scale. [Few comments: 1. We have a movie in the supplementary material. 2. Does the error also have the right slope? 3. We can put more images to exemplify the progress 4. Need to improve the micrograph's generation code]

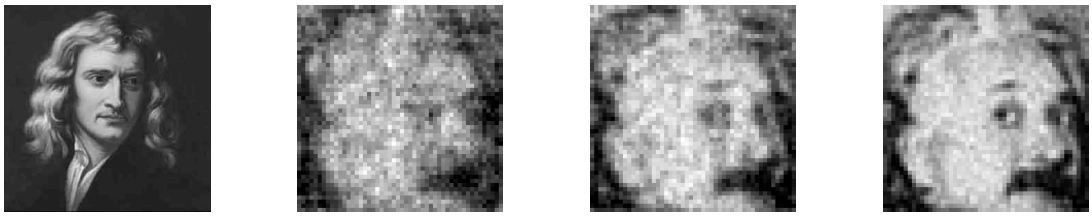

(a) Newton (model) (b) $P = 1024$ (c) $P = 1024 \times 10$ (d) $P = 1024 \times 100$

Figure 2: [Caption and image not yet revised] Recovery of Einstein's image. The RRR algorithm is initialized with the image of the physicist Issac Newton in the left panel. We show estimations of Einstein using $P = 1024, 1024 \times 10$ and 1024×100 number of micrographs, each contains 700 image occurrences on average and the SNR is $1/20$. The signal's estimation RMSE is 0.5514, 0.3494 and 0.2112, respectively. The power spectrum estimation RMSE is, respectively, 0.0269, 0.0083 and 0.0027. [Can add more images to exemplify the progress][Resolution of Newton too high?]

Results from a similar experiment with three ($K = 3$) one-dimensional signals are presented in Figure 4. We define the ratio of the space occupied by the ith signal as

$$\gamma_i = \frac{M_i L}{N}, \tag{2.2}$$

where M_i is the number of signal's occurrences, L is the length of the signal and N is the micrograph length. These ratios present the density of the the signals in the data. In the experiment, we do not assume to know these ratios, neither the noise level σ.

In order to estimate the signals, we computed the first three autocorrelation functions of the data and then estimated the signals and their corresponding γ_i using a nonconvex least-squares. As can be seen, given enough signal occurrences, we can estimate accurately the signals. The estimation quality of the triangle signal is poorer than the other two signals, a phenomenon that is explained using Proposition C.1. [1. We will replace the figure with a "progress figure" (like we did for Einstien) for each signals and a plot of the recovery error for all three signals. 2. We may want to replace the triangle signal]

3 Discussion

All current algorithmic pipeline for SPR using cryo–EM start with a particle picking algorithm which is prone to model bias. Bypassing the particle picking stage and constructing a 3-D model directly from the data—without assuming prior knowledge on the particle to be estimated—can be used to reconstruct ab initio models to initialize a refinement algorithm. Alternatively, it can be applied to generate templates for a particle picker which does not suffer from model bias.

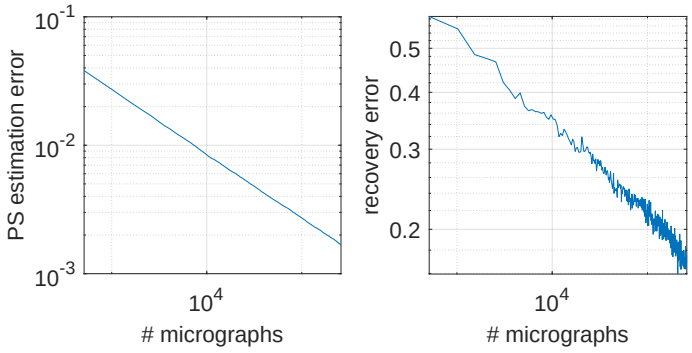

Figure 3: The left panel shows the RMSE of estimating the power spectrum of the signal from the data as a function of the number of collected micrographs. As expected, the curve is linear with slope $-1/2$ in logarithmic scale. The right panel shows the RMSE (in logarithmic scale) of recovering Einstein's image. [The program still runs so these figures will be extended to the right (more micrographs).]

In this paper, we examined a simplified model that, we believe, captures important features of the SPR problem. While the field is currently dominated by Bayesian methods such as EM, they are intractable for such problems. As an alternative, we propose to use autocorrelation analysis technique that shares some common lines (did you get the wordplay?) with Kam's method for ab inito modeling [29, 33, 45]. That being said, the SPR model is far more complicated than the model presented here. In a future research, we hope to bridge this gap.

Our results rely on two core assumptions that are not necessarily met by an SPR experiment. First, we modeled the background information as i.i.d. additive noise. In practice, the background information may be structured or signal dependent. Second, we assumed that the signal occurrences are all separated by the length of the signal, see (4.2). This separation can be induced by careful experimental design [???]. If the signals are not separated, one can introduce a new variable that represents the distribution of the spacing between signal occurrences and then compute explicitly the relation between the autocorrelation functions of the data and the signals. It is yet to be studied under what conditions on this distribution one can estimate the signals.

4 Methods

Mathematical model. Let $x_1, \dots, x_K \in \mathbb{R}^L$ be the sought signals and let $y \in \mathbb{R}^N$ be the data. The forward model can be posed as a mixture of *blind deconvolution* problems between

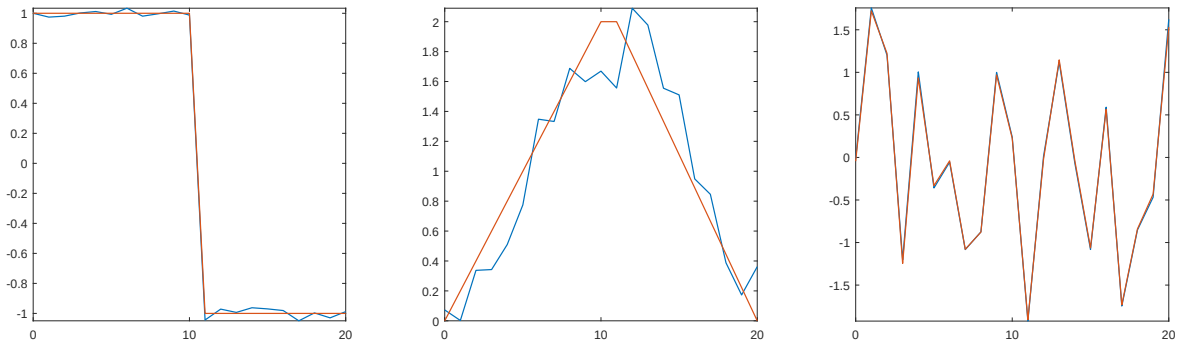

Figure 4: An experiment for estimate three one-dimensional signals simultaneously with noise level $\sigma = 3$. Red signals are the ground truth (targets) and the blue signals are our estimations. Individual RMSE of the estimates: 0.0239393/0.208925/0.0335956. The estimated γ's are 0.02574/0.01693/0.00818 and the true ones 0.02561/0.01707/0.00853. The SNR is 1/12. [1. to replace with a "progress" plot 2. replace the triangle signal 3. add error progress figure]

binary signals and the target signals x_i:

$$y = \sum_{i=1}^{K} x_i * s_i + \varepsilon, \quad \varepsilon \sim \mathcal{N}(0, \sigma^2 I). \tag{4.1}$$

The nonzero values of each $s_i \in \{0,1\}^N$ determine the position of x_i's occurrences. We denote the set of these nonzero values by $\mathcal{S}_i$ and its cardinality by $|\mathcal{S}_i| = M_i$. By assuming that all $\mathcal{S}_i$'s are disjoint, we let $s = \sum_{i=1}^{K} s_i$, $\mathcal{S} = \bigcup_{i=1}^{K} \mathcal{S}_i$ and $|\mathcal{S}| := M = \sum_{i=1}^{K} M_i$. Literature survey on blind deconvolution and related problems is given in Appendix B.

In order to estimate the mixture of autocorrelations, we assume that the support of s is not clustered. In particular, we assume that

$$|i - j| \geq L - 1, \quad \text{for all } i, j \in \mathcal{S} \text{ such that } i \neq j. \tag{4.2}$$

The goal of the problem is to estimate $x_1, \ldots, x_K$ from y.

Aperiodic autocorrelation functions For $z \in \mathbb{R}^L$ and $k \geq 2$, the autocorrelation of order k is defined for any integer shifts $\ell_1, \ldots, \ell_{k-1}$ by

$$a_z^k[\ell_1, \ldots, \ell_{k-1}] = \sum_{i=-\infty}^{+\infty} z[i] z[i + \ell_1] \ldots z[i + \ell_{k-1}], \tag{4.3}$$

where indexing of z out of the bounds $0, \ldots, L-1$ is zero-padded, as usual. Explicitly, the mean (which can be thought of as a first-order autocorrelation) and the second and third

autocorrelations are given by

$$\begin{aligned} a_z^1 &= \sum_{i=0}^{L-1} z[i], \\ a_z^2[\ell] &= \sum_{i=\max\{0,-\ell\}}^{L-1+\min\{0,-\ell\}} z[i]z[i+\ell], \\ a_z^3[\ell_1,\ell_2] &= \sum_{i=\max\{0,-\ell_1,-\ell_2\}}^{L-1+\min\{0,-\ell_1,-\ell_2\}} z[i]z[i+\ell_1]z[i+\ell_2]. \end{aligned} \tag{4.4}$$

Note that the autocorrelation functions are symmetric so that $a_z^2[\ell] = a_z^2[-\ell]$ and also

$$a_z^3[\ell_1,\ell_2] = a_z^3[\ell_2,\ell_1] = a_z^3[-\ell_1,\ell_2-\ell_1].$$

Estimating the autocorrelation function of a single signal. We first consider the problem of estimating the autocorrelations of a single signal from the data. The main principles carry through for $K > 1$ as will be shown next.

For the purpose of the analysis, we consider the asymptotic regime where $M, N \to \infty$, while preserving fixed ratio. Specifically, we define the ratio of the measurement occupied by the signal as

$$\gamma = \frac{ML}{N}. \tag{4.5}$$

Under the spacing constraint (4.2), we have $\gamma \leq \frac{L}{2L-1} \approx 1/2$.

The main pillar of this work is the following simple observation. If the support signal s satisfies the spacing constraint (4.2), then the first L entries of the data autocorrelations converge to a scaled, biased, version of the signal's autocorrelation:

$$\begin{aligned} \lim_{N\to\infty} a_y^1 &= \gamma a_x^1, \\ \lim_{N\to\infty} a_y^2[\ell] &= \gamma a_x^2[\ell] + \sigma^2\delta[\ell], \\ \lim_{N\to\infty} a_y^3[\ell_1,\ell_2] &= \gamma a_x^3[\ell_1,\ell_2] + \sigma^2\gamma a_x^1\big(\delta[\ell_1,0] + \delta[0,\ell_2] + \delta[\ell_1,\ell_2]\big), \end{aligned} \tag{4.6}$$

for $\ell, \ell_1, \ell_2 = 0, \ldots L-1$, and where δ denotes the Kronecker delta function.

Estimating the autocorrelation function of a multiple signals. As before, we consider the asymptomatic regime where $M_1, \ldots, M_K, N \to \infty$, while preserving fixed ratios

$$\gamma_k = \frac{M_k L}{N}, \quad \gamma = \sum_{k=1}^{K} \gamma_k. \tag{4.7}$$

If the support s satisfies the spacing constraint (4.2), then similarly to (4.6) one can estimate the mixture of the K signals' autocorrelations:

$$\begin{aligned}
\lim_{N\to\infty} a_y^1 &= \sum_{k=1}^{K} \gamma_k a_{x_k}^1, \\
\lim_{N\to\infty} a_y^2[\ell] &= \sum_{k=1}^{K} \gamma_k a_{x_k}^2[\ell] + \sigma^2\delta[\ell], \\
\lim_{N\to\infty} a_y^3[\ell_1,\ell_2] &= \sum_{k=1}^{K} \gamma_k a_{x_k}^3[\ell_1,\ell_2] + \sigma^2 \left(\sum_{k=1}^{K} \gamma_k a_{x_k}^1\right)(\delta[\ell_1,0]+\delta[0,\ell_2]+\delta[\ell_1,\ell_2]),
\end{aligned} \tag{4.8}$$

This relation is proven in Appendix A.

Numerical experiments details. For the 2-D experiment shown in Figures 2 and 3, we generated P micrographs of size 4096×4096 pixels. In each micrograph, we placed Einstein's image of size 50×50 in random locations, while keeping the separation condition (4.2). This is done by randomly selecting 4000 placements in the micrograph, one at a time with an accept/reject rule based on the separation constraint and locations picked so far. In average, 700 images were placed in each micrograph. Then, an i.i.d. Gaussian noise with standard deviation $\sigma = 3$ was added inducing SNR of approximately 1/20. An example of a micrograph's excerpt is presented in the right panel of Figure 1.

In this experiment, we assume to know the number of Einstein's occurrences and the noise level. In this situation, the second-order autocorrelation (or, equivalently, the Fourier magnitudes of the signal) determines almost all images uniquely up to reflection through the origin [23, 9]. Therefore, we estimate the signal's Fourier magnitude from the Fourier magnitude of the micrographs, in the cost of one FFT per micrograph. To estimate the signal, we use a phase retrieval algorithm called relaxed-reflect-reflect (RRR) that iterates by

$$z \to z + \beta(P_2(2P_1(z) - z) - P_1(z)), \tag{4.9}$$

where we set $\beta = 1$. RRR estimates a $2L \times 2L$ image. Exact solution contains Einstein's image in the upper-left corner and zero else where. The operator $P_2(z)$ combines the Fourier phases of the current estimation z with the Fourier magnitudes of the signal (estimated from the data). The operator $P_1(z)$ zeros out all entries of z outside the $L \times L$ upper-left corner. In order to compare the performance in multiple cases and different noise levels, the algorithm stopped after a fixed number of 1000 iterations and the iteration with the smallest error compared to the ground truth (also taking into account the reflection ambiguity) was chosen as the solution. While this cannot be done in practice since we do not have access to the ground truth, this procedure enables us to compare a large number of instances in different noisy environments [Note the last two sentences!].

For the 1-D experiment, we worked with three signals of length $L = 21$ and generated the data in the same way as in the 2-D example. The only difference is that here, for each placement, one of the three signals is picked at random proportionally to the desired number of occurrences of each. In this experiment, we computed the first three autocorrelation functions. We do not assume to know the number of occurrences of each signal γ_i ahead and we removed

the biased terms (see (4.6)) so we do not need to know σ either. In Appendix C we provide an argument on the number of equations we get from the first three autocorrelation functions.

To estimate the signal, we employ an optimization algorithm on the following nonlinear least-squares problem that estimate the signals and their number of occurrences simultaneously:

$$\min_{\substack{\hat{x}_1,\dots,\hat{x}_K\in\mathbb{R}^W \\ \hat{\gamma}_1,\dots,\hat{\gamma}_K>0}} w_1\left(a_y^1-\sum_{k=1}^K \hat{\gamma}_k a_{\hat{x}_k}^1\right)^2 + w_2\sum_{\ell=1}^{L-1}\left(a_y^2[\ell]-\sum_{k=1}^K \hat{\gamma}_k a_{\hat{x}_k}^2[\ell]\right)^2 + w_3\sum_{\substack{2\le\ell_1\le L-1 \\ 1\le\ell_2\le\ell_1-1}}\left(a_y^3[\ell_1,\ell_2]-\sum_{k=1}^K \hat{\gamma}_k a_{\hat{x}_k}^3[\ell_1,\ell_2]\right)^2. \quad (4.10)$$

where $W \geq L$ is the length of the sought signals and $w_1 = \frac{1}{2}, w_2 = \frac{1}{2}(L-1), w_3 = \frac{1}{(L-1)(L-2)}$; see [15] see for discussion on how to choose the weights properly.

Setting $W = L$ (as is a priori desired) is problematic because the above optimization problems appears to have numerous poor local optimizers. Thus, we first run the optimization with $W = 2L-1$. This problem appears to have fewer poor local optima, perhaps because the additional degrees of freedom allow for more escape directions. Since we hope the signals estimated this way correspond to the true signals zero-padded to length W, we extract from each one a subsignal of length L whose autocorrelation functions are the closest the measured ones in the sense of (4.10). This estimator is then used as initial iterate for (4.10), this time with $W = L$. We find that this procedure is reliable for a wide range of experimental parameters. To solve (4.10), we run the trust-region method implemented in Manopt [14], which allows to treat the positivity constraints [reference] on coefficients $\hat{\gamma}_k$. Notice that the cost function is a polynomial in the variables, so that it is straightforward to compute it and its derivatives.

References

[1] Emmanuel Abbe, Tamir Bendory, William Leeb, João Pereira, Nir Sharon, and Amit Singer. Multireference alignment is easier with an aperiodic translation distribution. *arXiv preprint arXiv:1710.02793*, 2017.

[2] Karim Abed-Meraim, Wanzhi Qiu, and Yingbo Hua. Blind system identification. *Proceedings of the IEEE*, 85(8):1310–1322, 1997.

[3] Cecilia Aguerrebere, Mauricio Delbracio, Alberto Bartesaghi, and Guillermo Sapiro. Fundamental limits in multi-image alignment. *IEEE Transactions on Signal Processing*, 64(21):5707–5722, 2016.

[4] Christophe Andrieu, Éric Barat, and Arnaud Doucet. Bayesian deconvolution of noisy filtered point processes. *IEEE Transactions on Signal Processing*, 49(1):134–146, 2001.

[5] GR Ayers and J Christopher Dainty. Iterative blind deconvolution method and its applications. *Optics letters*, 13(7):547–549, 1988.

[6] Jean-Marc Azais, Yohann De Castro, and Fabrice Gamboa. Spike detection from inaccurate samplings. *Applied and Computational Harmonic Analysis*, 38(2):177–195, 2015.

[7] Robert Beinert and Gerlind Plonka. Ambiguities in one-dimensional discrete phase retrieval from fourier magnitudes. *Journal of Fourier Analysis and Applications*, 21(6):1169–1198, 2015.

[8] Tamir Bendory. Robust recovery of positive stream of pulses. *IEEE Transactions on Signal Processing*, 65(8):2114–2122, 2017.

[9] Tamir Bendory, Robert Beinert, and Yonina C Eldar. Fourier phase retrieval: Uniqueness and algorithms. In *Compressed Sensing and its Applications*, pages 55–91. Springer, 2017.

[10] Tamir Bendory, Nicolas Boumal, Chao Ma, Zhizhen Zhao, and Amit Singer. Bispectrum inversion with application to multireference alignment. *arXiv preprint arXiv:1705.00641*, 2017.

[11] Tamir Bendory, Shai Dekel, and Arie Feuer. Robust recovery of stream of pulses using convex optimization. *Journal of Mathematical Analysis and Applications*, 442(2):511–536, 2016.

[12] Albert Benveniste, Maurice Goursat, and Gabriel Ruget. Robust identification of a nonminimum phase system: Blind adjustment of a linear equalizer in data communications. *IEEE Transactions on Automatic Control*, 25(3):385–399, 1980.

[13] Brett Bernstein and Carlos Fernandez-Granda. Deconvolution of point sources: A sampling theorem and robustness guarantees. *arXiv preprint arXiv:1707.00808*, 2017.

[14] N. Boumal, B. Mishra, P.-A. Absil, and R. Sepulchre. Manopt, a Matlab toolbox for optimization on manifolds. *Journal of Machine Learning Research*, 15:1455–1459, 2014.

[15] Nicolas Boumal, Tamir Bendory, Roy R Lederman, and Amit Singer. Heterogeneous multireference alignment: a single pass approach. *arXiv preprint arXiv:1710.02590*, 2017.

[16] Olivier Cappé, Arnaud Doucet, Marc Lavielle, and Eric Moulines. Simulation-based methods for blind maximum-likelihood filter identification. *Signal processing*, 73(1-2):3–25, 1999.

[17] Quentin Denoyelle, Vincent Duval, and Gabriel Peyré. Support recovery for sparse superresolution of positive measures. *Journal of Fourier Analysis and Applications*, 23(5):1153–1194, 2017.

[18] Joachim Frank and Terence Wagenknecht. Automatic selection of molecular images from electron micrographs. *Ultramicroscopy*, 12(3):169–175, 1983.

[19] Georgios B Giannakis and Jerry M Mendel. Identification of nonminimum phase systems using higher order statistics. *IEEE Transactions on Acoustics, Speech, and Signal Processing*, 37(3):360–377, 1989.

[20] Robert M Glaeser. Electron crystallography: present excitement, a nod to the past, anticipating the future. *Journal of structural biology*, 128(1):3–14, 1999.

[21] Sandeep Gogineni, Pawan Setlur, Muralidhar Rangaswamy, and Raj Rao Nadakuditi. Passive radar detection with noisy reference channel using principal subspace similarity. *IEEE Transactions on Aerospace and Electronic Systems*, 2017.

[22] George Harauz and Amelia Fong-Lochovsky. Automatic selection of macromolecules from electron micrographs by component labelling and symbolic processing. *Ultramicroscopy*, 31(4):333–344, 1989.

[23] MHMH Hayes. The reconstruction of a multidimensional sequence from the phase or magnitude of its fourier transform. *IEEE Transactions on Acoustics, Speech, and Signal Processing*, 30(2):140–154, 1982.

[24] Monson H Hayes and James H McClellan. Reducible polynomials in more than one variable. *Proceedings of the IEEE*, 70(2):197–198, 1982.

[25] Ayelet Heimowitz, Amit Singer, et al. Apple picker: Automatic particle picking, a low-effort cryo-em framework. *arXiv preprint arXiv:1802.00469*, 2018.

[26] Richard Henderson. The potential and limitations of neutrons, electrons and X-rays for atomic resolution microscopy of unstained biological molecules. *Quarterly reviews of biophysics*, 28(2):171–193, 1995.

[27] Richard Henderson. Avoiding the pitfalls of single particle cryo-electron microscopy: Einstein from noise. *Proceedings of the National Academy of Sciences*, 110(45):18037–18041, 2013.

[28] Stuart M Jefferies and Julian C Christou. Restoration of astronomical images by iterative blind deconvolution. *The Astrophysical Journal*, 415:862, 1993.

[29] Zvi Kam. The reconstruction of structure from electron micrographs of randomly oriented particles. *Journal of Theoretical Biology*, 82(1):15–39, 1980.

[30] Maryam Khoshouei, Mazdak Radjainia, Wolfgang Baumeister, and Radostin Danev. Cryo-EM structure of haemoglobin at 3.2 å determined with the Volta phase plate. *Nature communications*, 8:16099, 2017.

[31] John Kormylo and J Mendel. Identifiability of nonminimum phase linear stochastic systems. *IEEE transactions on automatic control*, 28(12):1081–1090, 1983.

[32] Robert Langlois, Jesper Pallesen, Jordan T Ash, Danny Nam Ho, John L Rubinstein, and Joachim Frank. Automated particle picking for low-contrast macromolecules in cryo-electron microscopy. *Journal of structural biology*, 186(1):1–7, 2014.

[33] Eitan Levin, Tamir Bendory, Nicolas Boumal, Joe Kileel, and Amit Singer. 3D ab initio modeling in cryo-em by autocorrelation analysis. *arXiv preprint arXiv:1710.08076*, 2017.

[34] Michael S Lewicki. A review of methods for spike sorting: the detection and classification of neural action potentials. *Network: Computation in Neural Systems*, 9(4):R53–R78, 1998.

[35] Yi-Lynn Liang, Maryam Khoshouei, Mazdak Radjainia, Yan Zhang, Alisa Glukhova, Jeffrey Tarrasch, David M Thal, Sebastian GB Furness, George Christopoulos, Thomas Coudrat, et al. Phase-plate cryo-EM structure of a class B GPCR–G-protein complex. *Nature*, 546(7656):118, 2017.

[36] KS Lii, M Rosenblatt, et al. Deconvolution and estimation of transfer function phase and coefficients for nongaussian linear processes. *The annals of statistics*, 10(4):1195–1208, 1982.

[37] Yuxi Liu, Shane Gonen, Tamir Gonen, and Todd O. Yeates. Near-atomic cryo-EM imaging of a small protein displayed on a designed scaffolding system. *Proceedings of the National Academy of Sciences*, 2018.

[38] Lennart Ljung. System identification. In *Signal analysis and prediction*, pages 163–173. Springer, 1998.

[39] Toshihiko Ogura and Chikara Sato. Automatic particle pickup method using a neural network has high accuracy by applying an initial weight derived from eigenimages: a new reference free method for single-particle analysis. *Journal of structural biology*, 145(1-2):63–75, 2004.

[40] Amelia Perry, Jonathan Weed, Afonso Bandeira, Philippe Rigollet, and Amit Singer. The sample complexity of multi-reference alignment. *arXiv preprint arXiv:1707.00943*, 2017.

[41] Lawrence R Rabiner. A tutorial on hidden markov models and selected applications in speech recognition. *Proceedings of the IEEE*, 77(2):257–286, 1989.

[42] Sjors HW Scheres. Semi-automated selection of cryo-em particles in relion-1.3. *Journal of structural biology*, 189(2):114–122, 2015.

[43] Ofir Shalvi and Ehud Weinstein. New criteria for blind deconvolution of nonminimum phase systems (channels). *IEEE Transactions on information theory*, 36(2):312–321, 1990.

[44] Maxim Shatsky, Richard J Hall, Steven E Brenner, and Robert M Glaeser. A method for the alignment of heterogeneous macromolecules from electron microscopy. *Journal of structural biology*, 166(1):67–78, 2009.

[45] Amit Singer. Mathematics for cryo-electron microscopy. *arXiv preprint arXiv:1803.06714*, 2018.

[46] Jitendra Tugnait. Identification of nonminimum phase linear stochastic systems. In *The 23rd IEEE Conference on Decision and Control*, number 23, pages 342–347, 1984.

[47] Marin van Heel. Finding trimeric HIV-1 envelope glycoproteins in random noise. *Proceedings of the National Academy of Sciences*, 110(45):E4175–E4177, 2013.

[48] Marin van Heel, Michael Schatz, and Elena Orlova. Correlation functions revisited. *Ultramicroscopy*, 46(1–4):307–316, 1992.

[49] NR Voss, CK Yoshioka, M Radermacher, CS Potter, and B Carragher. Dog picker and tiltpicker: software tools to facilitate particle selection in single particle electron microscopy. *Journal of structural biology*, 166(2):205–213, 2009.

[50] Alex Wein. *Statistical Estimation in the Presence of Group Actions*. PhD thesis, 2018.

[51] Yanan Zhu, Qi Ouyang, and Youdong Mao. A deep learning approach to single-particle recognition in cryo-electron microscopy. *arXiv preprint arXiv:1605.05543*, 2016.

A Proof of (4.8)

Throughout the proof, we consider the case of one signal $K = 1$. The extension to $K > 1$ is straightforward by averaging the contributions of all signal with appropriate weights; see [15].

We will let the number of instances of the signal M grow with N, and write $M = M_N$ to emphasize this. We assume M_N grows proportionally with N, and define:

$$\gamma = \lim_{N\to\infty} \frac{M_N L}{N} < 1. \tag{A.1}$$

We will assume that $M_N = \Omega(N)$, so that $\gamma > 0$. In the sequel, we will suppress the explicit dependence of M on N for notational convenience.

We start by considering the mean of the data:

$$a_y^1 = \frac{1}{N}\sum_{i=0}^{N-1} y[i] = \frac{1}{N/L}\sum_{j=0}^{M-1}\frac{1}{L}\sum_{i=0}^{L-1} x[i] + \underbrace{\frac{1}{N}\sum_{i=0}^{N-1}\varepsilon[i]}_{\text{noise term}} \xrightarrow{a.s.} \gamma a_x^1, \tag{A.2}$$

where the noise term converges to zero almost surely (a.s.) by the strong law of large numbers.

We proceed with the (second-order) autocorrelation for fixed $\ell \in [0, \dots, L-1]$. We can compute:

$$\begin{aligned} a_y^2[\ell] &= \frac{1}{N}\sum_{i=0}^{N-1-\ell} y[i]y[i+\ell] \\ &= \underbrace{\frac{1}{N}\sum_{j=1}^{M}\sum_{i=0}^{L-\ell-1} x[i]x[i+\ell]}_{\text{signal term}} + \underbrace{\frac{1}{N}\sum_{i=0}^{N-1-\ell}\varepsilon[i]\varepsilon[i+\ell]}_{\text{noise term}} + \underbrace{\frac{1}{N}\sum_{j=1}^{M}\sum_{i=0}^{L-1} x[i]\varepsilon[s_j+i+\ell]}_{\text{cross-term}}. \end{aligned} \tag{A.3}$$

The cross-terms are linear in the noise, and are easily shown to vanish almost surely in the limit $N \to \infty$, by the strong law of large numbers. As for the signal term, we break it into M different sums, each containing one copy of the signal. This gives:

$$\frac{1}{N}\sum_{j=1}^{M}\sum_{i=0}^{L-\ell-1} x[i]x[i+\ell] = \frac{ML}{N}\frac{1}{L}\sum_{i=0}^{L-\ell-1} x[i]x[i+\ell] \xrightarrow{N\to\infty} \gamma a_x^2[\ell]. \tag{A.4}$$

We next analyze the pure noise term. When $\ell \neq 0$, we can break the noise term into a sum of independent terms:

$$\frac{1}{N}\sum_{i=0}^{N-1-\ell}\varepsilon[i]\varepsilon[i+\ell] = \frac{1}{\ell}\sum_{i=0}^{\ell-1}\frac{1}{N/\ell}\sum_{j=0}^{N/\ell-1}\varepsilon[j\ell+i]\varepsilon[(j+1)\ell+i]. \tag{A.5}$$

Each sum $\frac{1}{N/\ell}\sum_{j=0}^{N/\ell-1}\varepsilon[j\ell+i]\varepsilon[(j+1)\ell+i]$ is an average of N/ℓ independent terms with expectation zero, and thus converges to zero almost surely as $N \to \infty$. If $\ell = 0$, then we have:

$$\frac{1}{N}\sum_{i=0}^{N-1}\varepsilon^2[i] \xrightarrow{a.s.} \sigma^2. \tag{A.6}$$

We now analyze the third-order autocorrelation. Let us fix $\ell_1 \geq \ell_2 \geq 0$. We have:

$$\begin{aligned}
a_y^3[\ell_1,\ell_2] &= \frac{1}{N}\sum_{i=0}^{N-1-\ell_1} y[i]y[i+\ell_1]y[i+\ell_2] \\
&= \underbrace{\frac{ML}{N}\frac{1}{M}\sum_{j=1}^{M}\frac{1}{L}\sum_{i=0}^{L-1-\ell_1} x[i]x[i+\ell_1]x[i+\ell_2]}_{(1)} + \underbrace{\frac{1}{N}\sum_{i=0}^{N-1-\ell_1}\varepsilon[i]\varepsilon[i+\ell_1]\varepsilon[i+\ell_2]}_{(2)} \\
&\quad + \underbrace{\frac{1}{N}\sum_{j=1}^{M}\sum_{i=0}^{L-1} x[i]\varepsilon[s_j+i+\ell_1]\varepsilon[s_j+i+\ell_2]}_{(3)} + \underbrace{\frac{1}{N}\sum_{j=1}^{M}\sum_{i=0}^{L-1}\varepsilon[s_j+i-\ell_1]x[i]\varepsilon[s_j+i+\ell_2-\ell_1]}_{(4)} \\
&\quad + \underbrace{\frac{1}{N}\sum_{j=1}^{M}\sum_{i=0}^{L-1}\varepsilon[s_j+i-\ell_2]\varepsilon[s_j+i+\ell_1-\ell_2]x[i]}_{(5)} + \underbrace{\frac{1}{N}\sum_{j=1}^{M}\sum_{i=0}^{L-\ell_1+\ell_2-1}\varepsilon[s_j+i]x[i+\ell_1-\ell_2]x[i]}_{(6)} \\
&\quad + \underbrace{\frac{1}{N}\sum_{j=1}^{M}\sum_{i=0}^{L-\ell_2-1} x[i]\varepsilon[s_j+i+\ell_1]x[s_j+i+\ell_2]}_{(7)} + \underbrace{\frac{1}{N}\sum_{j=1}^{M}\sum_{i=0}^{L-\ell_1-1} x[i]x[i+\ell_1]\varepsilon[s_j+i+\ell_2]}_{(8)}.
\end{aligned} \tag{A.7}$$

Terms (6), (7) and (8) are linear in ε, and can easily be shown to converge to 0 almost surely by the law of large numbers, by similar arguments as used previously. Term (1) converges to $\gamma a_x^3[\ell_1,\ell_2]$ almost surely, for the same reasons as (A.4). To deal with terms (2)–(5), we must distinguish between different values of ℓ_1 and ℓ_1.

Case 1: $0 < \ell_2 < \ell_1$. Here, all summands with elements of ε involve products of distinct entries, which have expected value 0. Consequently, the usual argument shows that terms (2)–(5) all converge to 0 almost surely as $N \to \infty$.

Case 2: $0 = \ell_2 < \ell_1$. Term (2) is an average of products of the form $\varepsilon[i]^2\varepsilon[i+\ell_1]$, which have mean zero; consequently, term (2) converges to 0 almost surely. The same argument as

for Case 1 shows that (3) and (5) also converge to 0. For term (4), we write:

$$\frac{1}{N}\sum_{j=1}^{M}\sum_{i=0}^{L-1}\varepsilon[s_j+i-\ell_1]x[i]\varepsilon[s_j+i+\ell_2-\ell_1]$$
$$=\frac{ML}{N}\frac{1}{L}\sum_{i=0}^{L-1}x[i]\frac{1}{M}\sum_{j=1}^{M}\varepsilon[s_j+i-\ell_1]^2\xrightarrow{N\to\infty}\gamma\frac{1}{L}\sum_{i=0}^{L-1}x[i]\sigma^2=\gamma a_x^1\sigma^2. \tag{A.8}$$

Case 3: $0<\ell_2=\ell_1$. An argument nearly identical to that for Case 2 shows that terms (2), (4) and (5) converge to 0, while term (3) converges to $\gamma a_x^1\sigma^2$.

Case 4: $0=\ell_2=\ell_1$. The same argument as for term (4) in Case 2 shows that terms (3), (4) and (5) all converge to $\gamma a_x^1\sigma^2$. Term (2) is an average of $\varepsilon[i]^3$, which is mean zero; consequently, it converges to 0.

This completes the proof of (4.8).

B Related work

System identification. For $K=1$, our problem can be interpreted as a special case of the system identification problem. Similarly to (4.1), the system identification forward model takes the form $y=x*w+\varepsilon$, where x is the unknown signal (the "system"), w is an unknown, random, input sequence, and ε is an additive noise. The goal of this problem is to estimate x, usually referred to as "identifying the system." The question of identifiability of x under this observation model is addressed for certain Gaussian and non-Gaussian w in [12, 31]. In the special case where $w\in\{0,1\}^N$, satisfying the spacing requirement (4.2), we obtain our model in the case of a single signal ($K=1$). The same observation model is used for blind deconvolution, a longstanding problem arising in a variety of engineering and scientific applications such as astronomy, communication, image deblurring, system identification and optics; see [28, 43, 5, 2], just to name a few. [ref this by Giannakis: [19]]

Likelihood-based methods. Likelihood-based methods estimate x as the maximizer of some function $f(x|y)$, where f is derived from the likelihood function of x given the observed signal y. For example, f may be the likelihood itself, or a related function with a similar form (leading to the class of "quasi-likelihood" methods). If some prior is assumed on x, then $f(x|y)$ can be taken to be the posterior distribution of x given the data; this is the simplest form of Bayesian inference.

Optimizing the function $f(x|y)$ exactly is often intractable, and thus heuristic methods are used instead. One proposed technique is to use Markov Chain Monte Carlo (MCMC) [16]. Another paper considers parameterized models for multiple distinct signals, as in our framework ($K>1$) [4]. Their proposed solution is an MCMC algorithm tailored for their specific parametrized problem.

In special cases, including the case where w is binary, expectation maximization (EM) has been used [16]. The EM method for discrete w is based upon a certain "forward-backward" procedure used in hidden Markov models [41]. However, the complexity of this procedure is nonlinear in N, and therefore its usage is limited for big data sets. Indeed, on each iteration of EM, a probability must be assigned to any feasible combination of positions for the current

signal estimate in M locations on the grid $\{1, \ldots, N\}$. In total, even when excluding forbidden combinations due to the spacing constraint, there are $O(N^M)$ such combinations, and the problem becomes computationally intractable when M grows with N and N is large.

Because likelihood methods are computationally expensive, methods based on recovery from moments, which are akin to our method, have also been previously used for system identification. Methods based on the third- and fourth-order moments are described and analyzed in [36, 19, 46].

C Theory

The impossibility of detection in low SNR. If x is known and $K = 1$, then the locations s_i can be estimated via linear programming in the high SNR regime [6, 17, 11, 8, 13]. However, in the low SNR regime, estimating the binary sparse signal s is impossible. To see this, suppose that an oracle provides us M windows of length $W > L$, each containing exactly one copy of x. Suppose too that the oracle provides us with x itself. That is to say, we get a series of windows of length W, each one containing a signal x at an unknown location; and our only task is to estimate the locations. This is an easier problem than detecting the support of s. Nevertheless, even this simpler problem is impossible in the low SNR regime [3]. Consequently, detecting the nonzero values of s is impossible in low SNR.

Estimating a signal from its third-order autocorrelation. A one-dimensional signal is determined uniquely by its second- and third-order autocorrelations. Indeed, since $z[0]$ and $z[L-1]$ are non-zero by definition, we have the formula:

$$z[k] = \frac{z[0]z[k]z[L-1]}{z[0]z[L-1]} = \frac{a_z^3[k, L-1]}{a_z^2[L-1]}. \tag{C.1}$$

In particular, we have proven the following proposition:

Proposition C.1. *Let $z \in \mathbb{R}^L$ and suppose that $z[0]$ and $z[L-1]$ are nonzero. Then z is determined uniquely from a_z^2 and a_z^3.*

Some remarks are in order. First, formula (C.1) is not numerically stable if $z[0]$ and/or $z[L-1]$ are close to 0. In practice, we recover z by fitting it to its autocorrelations using a nonconvex least-squares procedures, which is empirically more robust to additive noise; we have seen similar phenomena for related problems [10, 15].

Second, if the spacing condition (4.2) holds, then the length of the signal can be determined from the autocorrelations. In particular, if (4.2) holds for some spacing $W \geq L$, then $a_z^2[i] = 0$ for all $i > L - 1$.

Note too that the second-order autocorrelation is not by itself sufficient to determine the signal uniquely [7, 9]. However, for dimensions greater than one, almost all signals are determined uniquely up to sign (phase for the complex signals) and reflection through the origin (with conjugation in the complex case) [23, 24]. The sign ambiguity can be resolved by the mean of the signal if it is not zero. However, determining the reflection symmetry still requires additional information, beyond the second-order autocorrelation.

Identifiability of parameters from the moments of y. The observed moments a_y^1, a_y^2 and a_y^3 of y do not immediately give the moments of the signal x, as seen by formula (4.6); rather, the two are related by the noise level σ and the ratio $\gamma = \lim_{N\to\infty} ML/N$, where $M = M_N$ grows with N. We will show, however, that x is still identifiable from the observed moments of y. In general, we say a parameter is "identifiable" if its value is uniquely determined in the limit $N \to \infty$.

First, we observe that if the noise level σ is known, one can estimate γ from the first two moments of the observed vector y.

Proposition C.2. *Let $K = 1$ and $\sigma > 0$ be fixed. If the mean of x is nonzero, then*

$$\gamma = \lim_{N\to\infty} \frac{(a_y^1)^2}{\sum_{j=0}^{L-1} a_y^2[j] - \sigma^2} \quad a.s.$$

Proof. The proof follows from plugging the explicit expressions of (4.6) into the right hand side of the equality. □

Using third-order autocorrelation information of y, both the ratio γ and the noise σ are identifiable. For the following results, when we say that a result holds for a "generic" signal x, we mean that it holds for all x inside a set $\Omega \subset \mathbb{R}^L$, whose complement $\mathbb{R}^L \setminus \Omega$ has Lebesgue measure zero.

Proposition C.3. *Let $K = 1$, and $\sigma > 0$ be fixed. Then, a_y^1, a_y^2 and a_y^3 determine the ratio γ and noise level σ uniquely for a generic signal x. If $\gamma \geq \frac{1}{4L(L-1)}$, then this holds for any signal x with nonzero mean.*

Proof. See Appendix D. □

From Propositions C.1 and C.3 we can directly deduce the following:

Corollary C.4. *Let $K = 1$ and $\sigma > 0$ be fixed. Then the signal x, the ratio γ, and the noise level σ are identifiable from the first three autocorrelation functions of y if:*

- *Either the signal x is generic; or*
- *Both $x[0]$ and $x[L-1]$ are nonzero, x has nonzero mean, and $\gamma \geq \frac{1}{4L(L-1)}$.*

Open theoretical questions. Our method of estimating x uses the third-order moments of the observations. These empirical moments are used to obtain consistent estimators of population parameters related to the the mean and second- and third-order autocorrelations of x, to which we fit the signal x. Consequently, the number of signal occurrences M should grow at least as fast as $1/\mathsf{SNR}^3$ to achieve a constant estimation error. In the related problem of multireference alignment [40, 1], this is optimal in the low SNR regime; we conjecture that the same is true for our problem.

Another interesting question is how many signals $x_1, \ldots, x_K$ can be demixed from their mixed autocorrelation functions. In [15], we empirically observed that $K \sim \sqrt{L}$ signals can be estimated simultaneously from their mixed second- and third-order autocorrelations, using the least-squares procedure. In [50] [TKTK: add reference to Alex Wein's thesis, or put personal correspondence], this result is shown theoretically for a different, and much less efficient, algorithm. In our current setting, the additional parameters γ and σ make the problem more challenging; however, we conjecture that the number of estimable signals still grows like $\sqrt{L}$.

D Proof of Proposition C.3

We will prove that both σ and γ are identifiable from the observed first three moments of y. For convenience, we will work with $\beta = \gamma/L$ rather than γ itself. We will construct two quadratic equations satisfied by β from observed quantities, independent of σ. Then, we will show that these equations are independent, and hence that β is uniquely defined. Given β, we can estimate σ using Proposition C.2.

Throughout the proof, it is important to distinguish between observed and unobserved values. We denote the observed values by E_i or a_y^1, a_y^2, a_y^3, while using F_i for functions of the signal's autocorrelations.

Recall that $a_y^1 = \beta(\mathbf{1}^T x)$ and and $a_y^2[0] = \beta\|x\|^2 + \sigma^2$, where $\mathbf{1} \in \mathbb{R}^L$ stands for vector of ones. Taking the product:

$$\begin{aligned} E_1 &:= a_y^1 a_y^2[0] = (\beta(\mathbf{1}^T x))(\beta\|x\|^2 + \sigma^2) \\ &= \sigma^2 a_y^1 + \beta^2 F_1, \end{aligned} \tag{D.1}$$

where $F_1 := a_x^3[0,0] + \sum_{j=1}^{L-1}(a_x^3[j,j] + a_x^3[0,j])$. The terms of F_1 can be also estimated from a_y^3, while taking the scaling and bias terms into account:

$$E_2 := \beta F_1 + (2L+1)\sigma^2 a_y^1. \tag{D.2}$$

Therefore, from (D.1) and (D.2) we get

$$E_2\beta - (2L+1)\sigma^2\beta a_y^1 = E_1 - \sigma^2 a_y^1. \tag{D.3}$$

Let $a_y^2 := \sum_{j=0}^{L-1} a_y^2[j]$ and recall from Proposition C.2:

$$\sigma^2 = a_y^2 - (a_y^1)^2/(\beta L). \tag{D.4}$$

Plugging into (D.3) and rearranging we get

$$\mathcal{A}\beta^2 + \mathcal{B}\beta + \mathcal{C} = 0, \tag{D.5}$$

where

$$\begin{aligned} \mathcal{A} &= E_2 - (2L+1)a_y^1 a_y^2, \\ \mathcal{B} &= -E_1 + \frac{2L+1}{L}(a_y^1)^3 + a_y^1 a_y^2, \\ \mathcal{C} &= -(a_y^1)^3/L. \end{aligned}$$

Importantly, these coefficients are observable quantities.

We are now proceeding to derive the second quadratic equation. We notice that

$$E_3 = \frac{1}{L}(a_y^1)^3 = \frac{1}{L}\beta^3(\mathbf{1}^T x)^3 = \frac{1}{L}\beta^3 F_2, \tag{D.6}$$

where

$$F_2 = a_x^3[0,0] + 3\sum_{j=1}^{L-1} a_x^3[j,j] + 3\sum_{j=1}^{L-1} a_x^3[0,j] + 6\sum_{1\le i<j\le L-1} a_x^3[i,j].$$

On the other hand, from a_y^3 we can directly estimate F_2 up to scale and bias

$$E_4 = \beta F_2 + (6L-3)\sigma^2 a_y^1. \tag{D.7}$$

Taking the ratio:

$$\frac{E_4}{E_3} = \frac{L}{\beta^2} + \frac{(6L-3)L\sigma^2 a_y^1}{E_3},$$

we conclude:

$$\sigma^2 = \frac{E_4}{a_y^1 L(6L-3)} - \frac{E_3}{\beta^2 a_y^1(6L-3)}.$$

Using (D.4) and rearranging we get the second quadratic:

$$\mathcal{D}\beta^2 + \mathcal{E}\beta + \mathcal{F} = 0, \tag{D.8}$$

where

$$\begin{aligned}
\mathcal{D} &= a_y^2 - \frac{E_4}{a_y^1 L(6L-3)}, \\
\mathcal{E} &= -(a_y^1)^2/L, \\
\mathcal{F} &= \frac{E_3}{a_y^1(6L-3)}.
\end{aligned}$$

To complete the proof, we need to show that the two quadratic equations (D.5) and (D.8) are independent. To this end, it is enough to show that the ratio between the coefficients is not the same. From (D.5) and (D.1), we have

$$\begin{aligned}
\frac{\mathcal{B}}{\mathcal{C}} &= \frac{LE_1 - (2L+1)(a_y^1)^3 - La_y^1 a_y^2}{(a_y^1)^3} \\
&= \frac{La_y^2[0] - (2L+1)(a_y^1)^2 - La_y^2}{(a_y^1)^2}.
\end{aligned}$$

In addition, using (D.6)

$$\frac{\mathcal{E}}{\mathcal{F}} = \frac{(3-6L)(a_y^1)^3}{LE_3} = 3 - 6L.$$

Now, suppose that the quadratics are dependent. Then, $\frac{\mathcal{B}}{\mathcal{C}} = \frac{\mathcal{E}}{\mathcal{F}}$, or,

$$La_y^2[0] - (2L+1)(a_y^1)^2 - La_y^2 = (a_y^1)^2(3-6L)$$

Rearranging the equation and writing in terms of x we get

$$4(L-1)\beta(a_x^1)^2 - \sum_{i=1}^{L-1} a_x^2[i] = 0. \tag{D.9}$$

For generic x, this polynomial equation is not satisfied. Therefore, the equations are independent. More than that, for any nonzero x, $(a_x^1)^2 > \sum_{i=1}^{L-1} a_x^2[i]$. Therefore, if $4(L-1)\beta \geq 1$, or,

$$\beta \geq \frac{1}{4(L-1)},$$

the condition (D.9) cannot be satisfied for any signal.

E Stuff

Many automatic and semi-automatic methods for particle picking have been proposed, based on edge detection, template matching and deep learning; see for instance [22, 39, 51, 18, 42, 25]. However, most of these procedures are prone to *model bias*. For instance, in the popular framework of RELION [42], the user manually marks hundreds of spots on the micrograph, believed to contain projections. Therefore, the algorithm's performance depends on the prior assumptions of the users about the particle's structure; the same holds true for deep learning based approaches which require constructing labeled sets of data. Other methods use disks or differences of Gaussians as templates [32, 49]. Nowadays, it also still popular to pick particles manually. This method, while it exploits the researcher's experience, is both tedious and subject to model bias.

F The autocorrelation functions in cryo–EM

The 3-D Fourier transform of an L-bandlimited 3-D volume (e.g., particle) can be expanded by spherical harmonics:

$$\hat{V}(k,\theta,\phi) = \sum_{\ell=0}^{L} \sum_{m=-\ell}^{\ell} A_{\ell,m}(k) Y_\ell^m(\theta,\phi), \tag{F.1}$$

where (θ,ϕ) are two angles on the sphere, k is the radial coordinate, $Y_\ell^m(\theta,\phi)$ is the spherical harmonic of degree ℓ and order m and $A_{\ell,m}(k)$ are the associated spherical harmonics coefficients, to be estimated. A rotation of the volume by $\omega \in SO(3)$ can be described using the Wigner D-function $D^\ell_{m,m'}$:

$$\begin{aligned}(R_\omega \hat{V})(k,\theta,\phi) &= \sum_{\ell=0}^{L} \sum_{m=-\ell}^{\ell} A_{\ell,m}(k) (R_\omega Y_\ell^m)(\theta,\phi) \\ &= \sum_{\ell=0}^{L} \sum_{m=-\ell}^{\ell} A_{\ell,m}(k) \sum_{m'=-\ell}^{m=\ell} D^\ell_{m,m'}(\omega) Y_\ell^{m'}(\theta,\phi).\end{aligned} \tag{F.2}$$

By the Fourier slice theorem, each cryo–EM measurement (projection) is equivalent (through 2-D Fourier transform) to the slice of $\hat{V}$, associated with $\theta = \pi/2$, after $\hat{V}$ was rotated by $\omega \in SO(3)$. Explicitly, the Fourier transform of a projection from the viewing direction ω is related to the spherical harmonic coefficients of the object through:

$$P_\omega(k,\phi) = \sum_{\ell=0}^{L} \sum_{m=-\ell}^{\ell} A_{\ell,m}(k) \sum_{m'=-\ell}^{m=\ell} D^\ell_{m,m'}(\omega) Y_\ell^{m'}(\pi/2,\phi). \tag{F.3}$$

Next, we want to relate the projections P_ω with the autocorrelation functions computed from the micrograph. We assume the projections are sufficiently separated so that the (Δ_x, Δ_y) entry of the second-order autocorrelation of the micrograph is proportional to:

$$M_2(\Delta_x,\Delta_y) \propto \sum_{n=1}^{N} \sum_{x,y} P_n(x,y) P_n(x+\Delta_x, y+\Delta_y) + \text{bias}, \tag{F.4}$$

where P_n denotes the nth projection. The assumption here is that (Δ_x, Δ_y) are small enough so that, in computing the auto-correlation, points (x, y) and $(x + \Delta_x, y + \Delta_y)$ do not touch distinct particles. By taking $n \to \infty$ and assuming uniform distribution of viewing directions, we get

$$M_2(\Delta_x, \Delta_y) \propto \sum_{x,y} \int_\omega P_\omega(x, y) P_\omega(x + \Delta_x, y + \Delta_y) d\omega. \tag{F.5}$$

In the same way and under the same conditions, the third moment is given by

$$M_3(\Delta_x^1, \Delta_y^1; \Delta_x^2, \Delta_y^2) \propto \sum_{x,y} \int_\omega P_\omega(x, y) P_\omega(x + \Delta_x^1, y + \Delta_y^1) P_\omega(x + \Delta_x^2, y + \Delta_y^2) d\omega + \text{bias}. \tag{F.6}$$

In order to determine the particle, by (F.1) one needs to estimate on the order of L^3 spherical harmonics coefficients. If the pixel size is proportional to $1/L$ (to match the volume's resolution), then M_3 provides on the order of L^4 equations involving triple products of P_ω. Since P_ω depends (after coordinate transformation) linearly in the spherical harmonic coefficients through (F.3), this means we have a system of $\sim L^4$ cubic equations in the $\sim L^3$ sought parameters. Importantly, the coefficients of these equations can be estimated from the micrographs directly, without particle picking stage.